Self-Optimizing Control of an LNG Liquefaction Plant

Adriaen Verheyleweghen, Johannes Jäschke*

Department of Chemical Engineering, Norwegian Univ. of Science and Technology (NTNU), Trondheim, NO-7491 (e-mail: verheyle@ntnu.no, jaschke@ntnu.no).

Abstract

In this paper we apply self-optimizing control (SOC) to a cascaded LNG liquefaction plant. We first introduce the model, and then define the operational objective, which is to achieve minimal energy consumption while satisfying operational constraints. Four control structures are compared; a "standard" temperature control structure, an SOC structure with two plant measurements, an SOC structure that uses a combination of plant measurements as controlled variable, and an SOC structure where we also include measurements of disturbances in addition to the plant measurements. We find that the SOC structures significantly reduce the average steady-state loss when the operating conditions change. We furthermore find that using more plant measurements in the SOC structure results in lowered losses. In particular, for the disturbances considered, the steady-state loss becomes acceptably low, such that there is no need for a supervisory real-time optimization layer. Finally, it has been found that including disturbance measurements results in somewhat reduced losses, although the improvement was insignificant for the studied case. The effectiveness of the SOC framework is shown by closed-loop step responses to selected disturbances.

Keywords: Self-optimizing control, LNG liquefaction, refrigeration cycle, optimal operation, control structure design

*Corresponding author

1. Introduction

Efficient energy use is a growing industrial challenge in today's competitive markets. This is especially true for large, energy-demanding processes such as refrigeration cycles used for the liquefaction of natural gas. Due to their significant power consumption, optimizing the operation of such processes is essential to reduce unnecessary energy usage [1].

Finding the optimal operation strategy of complex processes is a non-trivial task, as the presence of disturbances, implementation errors, changing operating conditions and non-linear system behavior must be addressed adequately. An increasingly popular method for achieving optimal operation at all times is "on-line optimization" [2]. On-line optimization, or economic model-predictive control (EMPC) [3], requires the repeated computation of an input trajectory by solving a (non-linear) optimization problem over a prediction horizon. Despite the advances in both software and hardware, there are still some drawbacks associated with these on-line methods. Depending on the complexity of the model, this dynamic optimization can be very computationally intensive. Another drawback may be that economic model predictive control requires a detailed and exact dynamic model of the process. Model-predictive control of refrigeration cycles is discussed in e.g. [4] and [5]. Specifically, the application of MPC to grocery refrigeration is discussed in [6, 7, 8].

A simpler approach to achieve optimal operation is to use traditional feedback control to control self-optimizing variables. It has been found that it is often possible to achieve acceptably small loss by controlling a combination of carefully chosen variables to a constant set-point [9, 10].

In this paper we design a self-optimizing control structure for an LNG liquefaction plant. The aim is to ensure near optimal operation under varying operating conditions and when the sensors are prone to measurement errors. The paper is an extension of [11], but instead of considering a single (multi-stage) refrigerant cycle, we consider multiple cascaded refrigerant cycles. Similar LNG liquefaction plants were also discussed in [12, 13, 14], where the authors discuss the optimal operating points and self-optimizing control strategies.

The main contributions of this paper are:

1. A model description of a cascaded LNG plant
2. The development and application of a different control structure for the LNG plant.

We apply the exact local method [15] to find the optimal combination of measurements for self-optimizing control, and show how measured disturbances can be used to augment the controlled variables to achieve better performance [16].

The optimal subset of measurements is found by a branch and bound method [17]. Finally, the derived control structures are compared with traditional temperature control and shown to be superior in terms of their steady-state losses.

The remainder of this paper is structured as follows: In section 2, we give a quick overview over self-optimizing control. In section 3, we introduce the model of the studied LNG plant. In section 4, we formulate the problem of optimal operation, and show the nominal solution thereof. The four different control structures are discussed in section 5. A comparison of the control structures in terms of their steady-state losses and their closed loop responses is shown in section 6. Finally, a discussion of the results and concluding remarks are given in section 7.

2. Self-optimizing control

A quick overview over self-optimizing control is given in this section. For a comprehensive review of the topic, see e.g. the survey paper by [10].

2.1. General principle

We assume that the problem of optimal operation can be formulated as an optimization problem

$$\min_{\bar{\mathbf{u}}} \quad J(\bar{\mathbf{u}}, \mathbf{d}) \tag{1a}$$

$$\text{s.t.} \quad g(\bar{\mathbf{u}}, \mathbf{d}) \leq 0, \tag{1b}$$

where $\bar{\mathbf{u}} \in \mathbb{R}^{n_{\bar{\mathbf{u}}}}$ are the inputs, $\mathbf{d} \in \mathbb{R}^{n_{\mathbf{d}}}$ are the disturbances, J is the scalar objective function and $g : \mathbb{R}^{n_{\bar{\mathbf{u}}} \times n_{\mathbf{d}}} \rightarrow \mathbb{R}^{n_g}$ denote the inequality constraints. Assuming further that the set of active constraints does not change, we can formally eliminate the active constraints and obtain an unconstrained optimization problem

$$\min_{\mathbf{u}} \quad J(\mathbf{u}, \mathbf{d}), \tag{2}$$

where, $\mathbf{u} \in \mathbb{R}^{n_{\mathbf{u}}}$ denote the remaining unconstrained degrees of freedom.

The purpose of self-optimizing control (SOC) is to achieve near-optimal operation by controlling carefully selected variables $\mathbf{c} \in \mathbb{R}^{n_{\mathbf{u}}}$ at their constant set-points [9]. If keeping these variables at their set-points results in an acceptably low loss during operation (in spite of varying disturbances), then self-optimizing control is achieved. In essence, we are trying to counteract the effect of unmeasured disturbances $\mathbf{d}$ by using feedback from the right combination of measurements.

The controlled variable $\mathbf{c}$ is often selected as a linear function of measurements

$$\mathbf{c} = \mathbf{H}\mathbf{y}, \tag{3}$$

or in terms of deviation variables

$$\Delta\mathbf{c} = \mathbf{H}\Delta\mathbf{y}, \tag{4}$$

where $\mathbf{H}$ is the selection matrix and $\mathbf{y}$ are the plant measurements. If $\mathbf{H}$ only has a single 1 as entry per row, we control single measurements. If the rows of $\mathbf{H}$ can take arbitrary values, we control a combination of measurements. A block diagram of the self-optimizing control structure is shown in Fig. 1

We choose the matrix $\mathbf{H}$ such that if we keep $\Delta\mathbf{c} = 0$, the loss is minimized. The loss is defined as the difference between the objective function evaluated at the current point and the optimal objective function value for that particular disturbance.

$$L = J(\mathbf{u}, \mathbf{d}) - J\left(\mathbf{u}^{\mathrm{opt}}, \mathbf{d}\right). \tag{5}$$

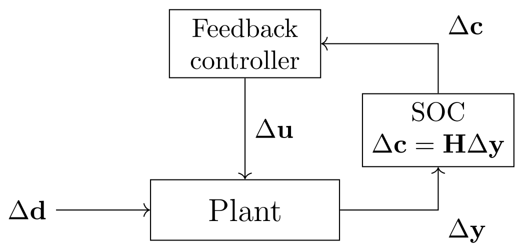

Figure 1: Block diagram of the self-optimizing control structure.

Evaluating the nonlinear loss function L for all possible control structures and disturbances is very computationally expensive. Therefore we approximate the nonlinear loss function (5) by a second order Taylor expansion around the optimal operating point [18]:

$$J(\mathbf{u},\mathbf{d}) \approx J(\mathbf{u}^{\mathrm{opt}},\mathbf{d}) + \mathbf{J}_{\mathbf{u}}(\mathbf{u}^{\mathrm{opt}},\mathbf{d})\Delta\mathbf{u} + \frac{1}{2}\Delta\mathbf{u}^{\intercal}\mathbf{J}_{\mathbf{uu}}(\mathbf{u}^{\mathrm{opt}},\mathbf{d})\Delta\mathbf{u}, \tag{6}$$

where $\mathbf{J}_{\mathbf{u}}(\mathbf{u}^{\mathrm{opt}})$ and $\mathbf{J}_{\mathbf{uu}}(\mathbf{u}^{\mathrm{opt}})$ are the Jacobian and Hessian of the objective, evaluated at the optimal point, respectively. Subtracting $J\left(\mathbf{u}^{\mathrm{opt}},\mathbf{d}\right)$ from both sides of (6), and taking into account that the gradient of the objective function $\mathbf{J}_{\mathbf{u}}\left(\mathbf{u}^{\mathrm{opt}},\mathbf{d}\right)$ is zero at the optimum, we obtain

$$\begin{aligned} L &= J\left(\mathbf{u},\mathbf{d}\right) - J\left(\mathbf{u}^{\mathrm{opt}},\mathbf{d}\right) && (7)\\ &\approx \frac{1}{2}\Delta\mathbf{u}^{\intercal}\mathbf{J}_{\mathbf{uu}}\Delta\mathbf{u}. && (8) \end{aligned}$$

2.2. Exact local method

In order to find the measurement selection matrix $\mathbf{H}$ that minimizes the loss, we need to be able to evaluate the loss for a given set of candidate control structures. The exact local method by Alstad et al. [15] allows us to to evaluate the average loss for a set of given disturbances and measurement noise.

We use a linearized plant model, in which the measurements $\mathbf{y}$ can be written as

$$\Delta\mathbf{y} = \mathbf{G}^{\mathbf{y}}\Delta\mathbf{u} + \mathbf{G}^{\mathbf{y}}_{\mathbf{d}}\mathbf{W}_{\mathbf{d}}\Delta\mathbf{d} + \mathbf{W}_{\mathbf{n}}\mathbf{n}. \tag{9}$$

Above, $\mathbf{W}_{\mathbf{n}^{\mathbf{y}}}$ and $\mathbf{W}_{\mathbf{d}}$ are diagonal matrices of appropriate sizes containing the variances of the measurement errors (noise) $\mathbf{n}$ and the disturbances $\mathbf{d}$, respectively. We assume further that both the measurement errors and the disturbances are normally distributed with known standard deviations and expected values.

Assuming the quadratic approximation of the loss in (8) is valid in a local neighbourhood of the optimal point, Kariwala et al. [19] show that the average loss can be expressed as

$$L_{avg} = \frac{1}{2} \left\| [\mathbf{M_d} \quad \mathbf{M_n}] \right\|_F^2 , \tag{10}$$

where $\|\cdot\|_F$ is used to denote the Frobenius norm, and where

$$\mathbf{M_d} = -\mathbf{J_{uu}}^{0.5} \left(\mathbf{H}\mathbf{G^y}\right)^{-1} \mathbf{H}\mathbf{F}\mathbf{W_d} \tag{11}$$

$$\mathbf{M_n} = -\mathbf{J_{uu}}^{0.5} \left(\mathbf{H}\mathbf{G^y}\right)^{-1} \mathbf{H}\mathbf{F}\mathbf{W_n}, \tag{12}$$

with the sensitivity matrix $\mathbf{F}$ is defined as [18]

$$\mathbf{F} = \frac{d\mathbf{y}^{\text{opt}}}{d\mathbf{d}} \tag{13}$$

$$= \mathbf{G^y_d} - \mathbf{G^y}\mathbf{J_{uu}}^{-1}\mathbf{J_{ud}}. \tag{14}$$

The optimal sensitivity matrix $\mathbf{F}$ describes the optimal change of the measurement $\mathbf{y}$ with respect to disturbances $\mathbf{d}$. We can then write

$$[\mathbf{M_d} \quad \mathbf{M_{n^y}}] = \mathbf{J_{uu}}^{1/2} \left(\mathbf{H}\mathbf{G^y}\right)^{-1} \mathbf{H}\mathbf{Y}, \tag{15}$$

where

$$\mathbf{Y} = [\mathbf{F}\mathbf{W_d} \quad \mathbf{W_{n^y}}] . \tag{16}$$

Putting everything together, we have that the selection matrix $\mathbf{H}$ that minimizes the average loss in (10) is

$$\mathbf{H} = \arg\min_{\mathbf{H}} = \left\| \mathbf{J_{uu}}^{1/2} \left(\mathbf{H}\mathbf{G^y}\right)^{-1} \mathbf{H}\mathbf{Y} \right\|_F . \tag{17}$$

An analytical solution of (17) is: [20]

$$\widetilde{\mathbf{H}}^\intercal = \left(\mathbf{Y}\mathbf{Y}^\intercal\right)^{-1} \mathbf{G^y}. \tag{18}$$

2.3. Inclusion of measured disturbances and optimal variations thereof

Sometimes it is easy and cheap to measure disturbance variables, and in that case they may be included into the measurement combination matrix $\mathbf{H}$. Including measurements of the disturbances in $\mathbf{H}$ may result in reduced loss [16]. The reason for this is that detailed knowledge of the system can be incorporated in the control structure, giving a proactive approach to disturbance rejection rather than a reactive one. This results in a combined feed-forward-feedback control structure.

Including the measured disturbances into an augmented measurement vector yields

$$\Delta\mathbf{y}^{\mathbf{aug}} = \begin{bmatrix} \Delta\mathbf{y} \\ \Delta\mathbf{d}^{\mathbf{m}} \end{bmatrix}, \tag{19}$$

and we can define the augmented linearized model

$$\Delta\mathbf{y}^{\mathbf{aug}} = \mathbf{G}^{\mathbf{y},\mathbf{aug}}\Delta\mathbf{u} + \mathbf{G}_{\mathbf{d}}^{\mathbf{y},\mathbf{aug}}\Delta\mathbf{d}^{\mathbf{aug}}, \tag{20}$$

where

$$\mathbf{G}^{\mathbf{y},\mathbf{aug}} = \begin{bmatrix} \mathbf{G}^{\mathbf{y}} \\ \mathbf{0}_{\mathbf{n}_{\mathbf{d}^{\mathbf{m}}}\cdot\mathbf{n}_{\mathbf{u}}} \end{bmatrix} \tag{21}$$

and

$$\mathbf{G}_{\mathbf{d}}^{\mathbf{y},\mathbf{aug}} = \begin{bmatrix} \mathbf{G}_{\mathbf{d}}^{\mathbf{y}} \\ \mathbf{I}_{\mathbf{d}^{\mathbf{m}}} \end{bmatrix}, \tag{22}$$

to select $\mathbf{H}$ with the previously described approach. The new controlled variable is then

$$\Delta\mathbf{c} = \mathbf{H}^{\mathbf{aug}}\Delta\mathbf{y}^{\mathbf{aug}}. \tag{23}$$

The variances of the measurement errors, $\mathbf{W}_{\mathbf{n}^{\mathbf{y}}}^{\mathbf{aug}}$ are

$$\mathbf{W}_{\mathbf{n}^{\mathbf{y}}}^{\mathbf{aug}} = \begin{bmatrix} \mathbf{W}_{\mathbf{n}^{\mathbf{y}}} & 0 \\ 0 & \mathbf{W}_{\mathbf{n}_{\mathbf{d}^{\mathbf{m}}}} \end{bmatrix}. \tag{24}$$

This can also be interpreted as a set-point adaptation scheme, where instead of keeping

$$\Delta\mathbf{c}^{\mathbf{aug}} = \mathbf{H}\Delta\mathbf{y} + \mathbf{H}^{\mathbf{d}}\Delta\mathbf{d}^{\mathbf{m}} = 0, \tag{25}$$

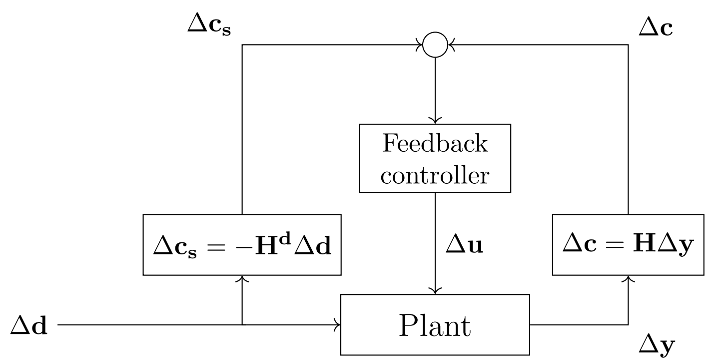

Figure 2: Block diagram of the set-point adaptation scheme for a self-optimizing control structure with measured disturbances, adapted from [10].

we instead control $\Delta\mathbf{c} = \mathbf{H}\Delta\mathbf{y}$ to the adapted set-point $\Delta\mathbf{c}_s = -\mathbf{H^d}\Delta\mathbf{d^m}$, as illustrated in Fig. 2 [10].

2.4. Selecting subsets of measurements

The expressions above (18) generate measurements combinations that include all available measurements. In practice, however, this is not necessary, as it is found that beyond a certain number of measurements, the loss does not decrease significantly [17]. On one hand, more measurements improve the accuracy (average loss) of the control structure, since the impact of disturbances and noise is reduced. On the other hand, every added sensor increases the investment cost and the chance of failure. The optimal set of measurements for a given control structure lies on a Pareto frontier, as illustrated in Fig. 3. Heuristics can give a good indication of which plant measurements to include when designing the control structure, but this approach requires system understanding and quickly becomes infeasible as the complexity of the plant grows. As an alternative, the best subset of measurements can be determined systematically using optimization. One such method is the branch and bound algorithm proposed by Kariwala et al. [17]. This method systematically selects the best subset of measurements, and will be used in this work. Another method to selected the optimal measurement set is by formulating the problem as an MIQP,

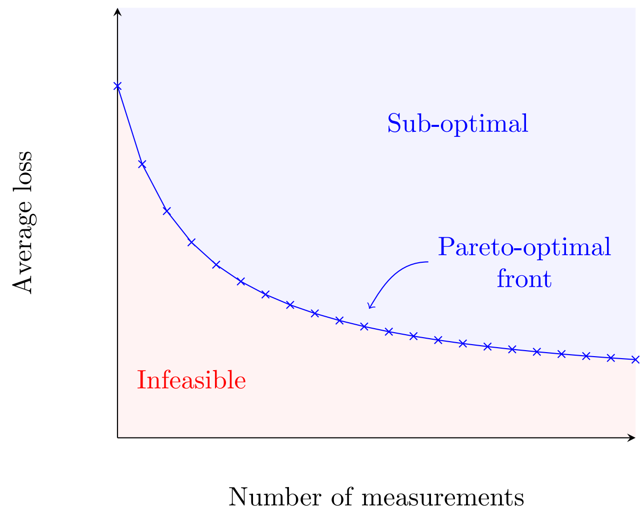

Figure 3: Illustration of average loss vs number of measurements for a self-optimizing control structure. The optimal set of a given number of measurements lies on the Pareto frontier.

where the integer variables indicate whether a measurement is active or not [20]. For the case studied in this paper, it was found that both methods found the same optimal solution, resulting in the same measurement sets.

3. Process description

The process studied in this work is a cascaded LNG refrigeration plant, similar to [21]. The operational goal is to cool the pretreated natural gas to a sufficiently low temperature such that it stays in liquid phase when the pressure is lowered to ambient pressure. A temperature of no higher than -150 °C is required to ensure this. After refrigeration, the LNG is sent to storage facilities.

The cascaded refrigeration plant consists of multiple, increasingly cold, closed cycles which exchange heat with each other. The advantage of such a design is that the mean temperature difference between the hot and cold streams can be kept small, resulting in lower energy consumption. This particular plant has three separate refrigerant cycles; propane, ethane and methane. An illustration of the full process is shown in Fig. 4.

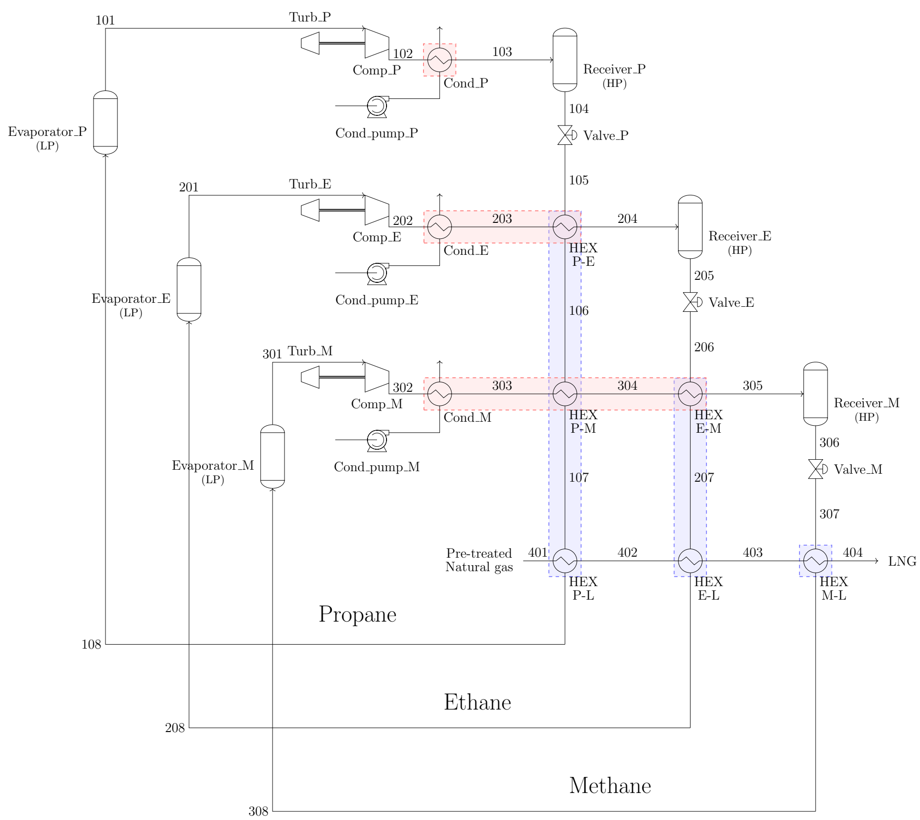

Figure 4: Process flow diagram of the studied process. It consists of three interconnected refrigeration cycles. P, E and M are used to refer to the refrigerants; propane, ethane and methane, respectively. HP and LP refer to the high and low pressure sides of the cycles. The condensing section of each cycle is indicated in red and the evaporation section is indicated in blue.

Each of the three cycles consists of a compressor, a condenser, an expansion valve and an evaporator. For simplicity, we assume that the compression occurs in a single-stage compressor. The compressor is driven by a turbine, which allows the compressor speed to be adjusted.

After compression, the superheated refrigerant enters the condensing section, in which the vapor is cooled and condensed using sea water. For a refrigeration plant consisting of 3 cascaded refrigerant cycles, the condensing section of the propane cycle can be modeled as a water-cooled condenser followed by a propane/ethane heat exchanger and a propane/methane heat exchanger. The ethane refrigerant enters the propane/ethane heat exchanger on the hot side of the exchanger and the ethane/methane heat exchanger on the cold side of the exchanger. In reality, heat is transferred in a large, multi-stream heat exchanger to avoid unnecessary investment cost and heat loss. However, for simplicity, we chose to model it as a series of two-stream heat exchangers.

On the low-pressure side of the cycle, the refrigerant is evaporated in a series of cross-cycle heat exchangers and an LNG heat exchanger.

In the following subsection, we describe the system model. To generalize and avoid unnecessary repetition of equations, we introduce the subscript $i \in \{\text{propane, ethane, methane}\}$ for the three refrigerants.

Model parameters for the various units are given in the Appendix B.

3.1. Thermodynamics

The enthalpies of gaseous and liquid refrigerant, their saturation temperatures and pressures are determined using the AllProps software [22], which utilizes the Helmholtz equation of state to calculate the thermodynamic properties. Surrogate models are fitted to the data calculated by AllProps and used in the optimization.

The saturation temperature is fitted to a model on the form

$$T_{\text{sat},i} = \sum_{j=0}^{2} c_{T_{\text{sat}},i,j} \log(P_i)^j, \tag{26}$$

where P_i is the pressure of refrigerant i, and $c_{T_{\mathrm{sat}},i,j}$ are the model parameters, which can be found in Tab. A.4. The specific saturation enthalpies of liquid and vapor phases are fitted to polynomial expressions on the form

$$\hat{H}_{\mathrm{liq},i} = \sum_{j=0}^{6} c_{\hat{H}_{\mathrm{liq},i,j}} P_i^j \tag{27}$$

$$\hat{H}_{\mathrm{vap},i} = \sum_{j=0}^{6} c_{\hat{H}_{\mathrm{vap},i,j}} P_i^j. \tag{28}$$

The coefficients $c_{H_{\mathrm{liq},i,j}}$ and $c_{\hat{H}_{\mathrm{vap},i,j}}$ are shown in Tab. A.5 and Tab. A.6. Heat capacities for vapor refrigerant i, $C_{p,i}$, are calculated as a function of temperature T_i

$$\frac{C_{p,i}}{R} = c_{C_{p,i},1} + c_{C_{p,i},2} T_i + c_{C_{p,i},3} T_i^2, \tag{29}$$

where R is the universal gas constant. The coefficients $c_{C_{p,i},j}$ are found in Tab. A.7. In the liquid phase, the heat capacities are assumed to be constant.

The compressibility factor Z_i is calculated using Dranchuk and Abou-Kassems equation of state [23].

$$\begin{aligned} Z_i = 1 &+ \left(c_{Z_i,1} + \frac{c_{Z_i,2}}{(T_{r,i})} + \frac{c_{Z_i,3}}{(T_{r,i})^3} + \frac{c_{Z_i,4}}{(T_{r,i})^4} + \frac{c_{Z_i,5}}{(T_{r,i})^5} \right) B \\ &+ \left(c_{Z_i,6} + \frac{c_{Z_i,7}}{(T_{r,i})} + \frac{c_{Z_i,8}}{(T_{r,i})^2} \right) B^2 \\ &- \left(\frac{c_{Z_i,7}}{(T_{r,i})} + \frac{c_{Z_i,8}}{(T_{r,i})^2} \right) c_{Z_i,9} B^5 \\ &+ c_{Z_i,10} \left(1 + c_{Z_i,11} B^2\right) \left(\frac{B^2}{T_{r,i}^3} \right) \exp\left(-c_{Z_i,11} B^2\right), \end{aligned} \tag{30}$$

where

$$B = \frac{0.27 P_{r,i}}{Z_i T_{r,i}}. \tag{31}$$

In the above equations, $T_{r,i}$ and $P_{r,i}$ are the reduced temperatures and pressures of the vapor, respectively. These are defined as

$$T_{r,i} = \frac{T_i}{T_{c,i}} \tag{32}$$

$$P_{r,i} = \frac{P_i}{P_{c,i}}, \tag{33}$$

where $T_{c,i}$ and $P_{c,i}$ are the critical temperatures and pressures. The coefficients for (30) can be found in Tab. A.8

3.2. Compressors

Polytropic compression models are used for the compressors. For a polytropic compressor, the following relationship is valid

$$\left(\frac{T_{discharge,i}}{T_{suction,i}}\right) = \left(\frac{P_{discharge,i}}{P_{suction,i}}\right)^{1/k_i}, \tag{34}$$

where the $T_{discharge,i}$, $T_{suction,i}$, $P_{discharge,i}$ and $P_{suction,i}$ are temperature and pressure at the compressor inlet and outlet, and k_i is the polytropic coefficient, which is defined as

$$k_i = \eta_i \frac{\gamma_i}{\gamma_i - 1}. \tag{35}$$

Here, η_i is the polytropic efficiency, and γ_i is the average adiabatic heat ratios at compressor discharge and suction:

$$\gamma_i = \frac{1}{2}\left(\frac{C_{p,suction,i}}{C_{p,suction,i} - R} + \frac{C_{p,discharge,i}}{C_{p,discharge,i} - R}\right) \tag{36}$$

The polytropic head is

$$h_{poly,i} = \frac{k_i Z_{suction,i} R}{g M_{m,i}} \left(T_{discharge,i} - T_{suction,i}\right), \tag{37}$$

where $Z_{suction,i}$ is the compressibility factor at the compressor inlet, R is the universal gas constant, g is the gravitational constant, $M_{m,i}$ is the molar mass,

The efficiencies η_i and compressor heads $h_{poly,i}$ are given by compressor maps, which are of the form

$$\eta_i = c_{\eta_i,1} h_{poly,scaled,i} + c_{\eta_i,2} - 10^{(c_{\eta_i,3} h_{poly,scaled,i} - c_{\eta_i,4})} \tag{38}$$

and

$$\frac{q_{suction}}{(u_i^{comp.})^{c_{comp,1}}} = \frac{c_{comp,2} h_{poly,scaled,i} - c_{comp,3}}{c_{comp,4}}, \tag{39}$$

where $q_{suction}$ is the suction volumetric flow rate, which can be expressed as

$$q_{suction,i} = \frac{\dot{n}_{suction,i} R T_{suction,i}}{P_{suction,i}}, \tag{40}$$

where $\dot{n}_{suction,i}$ is the molar flow rate of refrigerant at the compressor inlet, and

$$h_{poly,scaled,i} = \frac{h_{poly,i}}{(u_i^{comp.})^{c_{h_{poly,scaled,i},1}}} \tag{41}$$

is the scaled compressor head. $u_i^{comp.} \in [0.6, 1.1]$ is the normalized compressor speed. The coefficients for the above equations are shown in Tab. A.9-A.11 in Appendix B.

3.3. Valves

The flow through the valves is given by the valve equation

$$\dot{n}_i = u_i^{valve} c_{choke,i} \sqrt{P_{out} - P_{in}} \tag{42}$$

where $c_{choke,i}$ is the valve constant, see Tab. A.12, and $u_i^{valve} \in [0, 1]$ is the valve opening.

3.4. Evaporators and condensers

Heat transfer in the evaporators and condensers is calculated using the logarithmic mean temperature difference method

$$\dot{Q}_i = UA_i \frac{\Delta T_1 - \Delta T_2}{\log \Delta T_1 - \log \Delta T_2} \tag{43}$$

$$= \dot{H}_{cold,out} - \dot{H}_{cold,in} \tag{44}$$

$$= \dot{H}_{hot,in} - \dot{H}_{hot,out}, \tag{45}$$

where

$$\Delta T_1 = T_{hot,in} - T_{cold,out}, \tag{46}$$

$$\Delta T_2 = T_{hot,out} - T_{cold,in}. \tag{47}$$

3.5. Dynamics

The dynamics of the system are introduced by the liquid receivers following the condensers. The dynamic energy balances of the three receivers can be

Table 1: Expected values of the disturbances and their standard deviations

Disturbance	Expected value	Std. deviation
T_{401}	20 [°C]	2 [°C]
$\dot{m}_{401}$	$3.074 \cdot 10^4$ [kgmole/h]	$1.5 \cdot 10^3$ [kgmole/h]
$T_{ambient}$	5 [°C]	1 [°C]
$UA_{cond,P}$	0.51 [-]	0.0255 [-]
$UA_{cond,E}$	0.45 [-]	0.0225 [-]
$UA_{cond,M}$	0.27 [-]	0.0135 [-]

written as

$$\frac{dT_{receiver,P}}{dt} = \frac{\dot{n}_{103}}{n_{receiver}} (T_{103} - T_{104}) \tag{48}$$

$$\frac{dH_{receiver,E}}{dt} = \dot{H}_{204} - \dot{H}_{205} = \dot{n}_{204}\hat{H}_{204} - \dot{n}_{205}\hat{H}_{205} \tag{49}$$

$$\frac{dH_{receiver,M}}{dt} = \dot{H}_{305} - \dot{H}_{306} = \dot{n}_{305}\hat{H}_{305} - \dot{n}_{306}\hat{H}_{306} \tag{50}$$

$$\tag{51}$$

We assume that the levels are perfectly controlled, thus simplifying the dynamic mass balances to algebraic equations.

4. Defining the optimization problem to find the nominal operating point

4.1. Expected disturbances

Under operation we assume that the following parameters can vary (disturbances): the inlet temperature T_{401} and flow rate $\dot{m}_{401}$ of the natural gas, the ambient water temperature $T_{ambient}$ in the condensers and the heat transfer efficiency UA of each of the three condensers. Lower efficiency in the heat exchangers could be caused by e.g. fouling. The expected magnitudes of the disturbances are shown in Tab. 1.

4.2. Operational degree of freedom analysis

Using the method described by Jensen and Skogestad [24] for identification of degrees of freedom in refrigeration cycles, this plant can be shown to have five potential steady-state degrees of freedom per cycle. These five degrees of freedom are

1. Compressor power
2. Choke valve opening
3. Active charge (the amount of refrigerant circulating in the refrigeration cycle)
4. Transferred heat in condenser
5. Transferred heat in evaporator

Adjusting the transferred heat in the evaporator can be achieved by adjusting the load, or by bypassing the heat exchanger. For a given load, however, it is usually optimal to utilize the heat exchanger to its full potential. Furthermore, our refrigeration cycle lacks a way to adjust the active charge, thus resulting in zero sub-cooling by design. The liquid receiver consequently contains saturated liquid. [25] show that this design, although very common in industry, is sub-optimal. This liquefaction plant therefore has three degrees of freedom per cycle, for a total of nine degrees of freedom.

4.3. Optimization problem for optimal nominal operation

The overall aim is to minimize the energy consumption of the liquefaction plant for a given LNG load. The nominal operating point is found by solving the energy-minimizing optimization problem. We define the objective as

$$J(\mathbf{u}) = \sum_i W_i^{compressor}, \tag{52}$$

where $W_i^{compressor}$ is the work performed by compressor i.

The optimization is subject to a number of operational constraints, which are summarized in Tab. 2

Table 2: Process constraints and variable bounds for the steady-state optimization problem.

Constraint	Explanation
$T_{404} \leq -150$ °C	Maximum LNG outlet temperature
$P_{i01} \geq 0.4$ bar	Minimum pressure in cycle
	$i = \{$propane, ethane, methane$\}$
$0.0 \leq u_i^{choke} \leq 1.0$	Bounds on normalized choke openings
	$i = \{$propane, ethane, methane$\}$
$0.0 \leq u_i^{cond.} \leq 0.5$	Bounds on normalized condenser flow rate
	$i = \{$propane, ethane, methane$\}$
$0.6 \leq u_i^{comp.} \leq 1.1$	Bounds on normalized comp. speeds
	$i = \{$propane, ethane, methane$\}$

4.4. Nominal solution

Given the cost function (52) and the constraints from Tab. 2, a nonlinear programming problem (NLP) was formulated and implemented in MATLAB using Casadi 3.0.0 [26] and solved using IPOPT 3.12.3 [27]. The nominal solutions of some key variables are shown in Tab. 3.

The nominal solution features four active constraints, namely:

1. Upper bound of the LNG outlet temperature

2-4. Maximum condenser duty in each cycle (3 constraints)

Our optimal solution is qualitatively similar to the one found by [13], but differs from [12] in that no lower pressure constraint is active. While [12] assumed a constant isentropic efficiency for the compressors, we have used compressor maps, as discussed in Sec. 3. As a result of this, optimal operation favors maximum efficiency, if permitted by the other operational constraints. Optimal efficiency is achieved at the compressor "sweet spot", which gives inactive pressure constraints.

At the optimal operating point, the overall compressor duty is 75 MW.

Table 3: Nominal values of key variables

Variable	Nominal value	Variable	Nominal value
T_{101}	-43.5 °C	T_{102}	41.4 °C
T_{103}	13.2 °C	T_{201}	-98.1 °C
T_{202}	79.6 °C	T_{203}	12.8 °C
T_{204}	-39.4 °C	T_{301}	-154.9 °C
T_{302}	82.8 °C	T_{303}	12.9 °C
T_{304}	-40.0 °C	T_{305}	-93.0 °C
T_{401}	20.0 °C	T_{402}	-42.8 °C
T_{403}	-92.3 °C	T_{404}	-150.0 °C
$p_{propane}^{low}$	0.89 bar	$p_{propane}^{high}$	6.95 bar
p_{ethane}^{low}	0.41 bar	p_{ethane}^{high}	7.90 bar
$p_{methane}^{low}$	1.76 bar	$p_{methane}^{high}$	33.25 bar
p_{LNG}^{low}	39.00 bar	p_{LNG}^{high}	39.00 bar
$W_{comp.}^{total}$	75 MW		

5. Control structure design

5.1. Active constraint control and stabilization

In each of the refrigeration cycles, all liquid inventories except one must be stabilized in accordance with Aske and Skogestads [28] rules for consistent inventory control, to avoid overfilling or draining the tank. For this purpose, we chose to use the chokes to control the levels of the liquid receivers after the condensers. The LNG outlet temperature is controlled using the methane compressor speed. The condenser duties in all three cycles are nominally maximized, resulting in the usage of three potential degrees of freedom. After controlling the active constraints and the levels, we are left with a total of two degrees of freedom for the entire liquefaction plant. An illustration of the process with the stabilizing control and active constraint control structures is shown in Fig. 5.

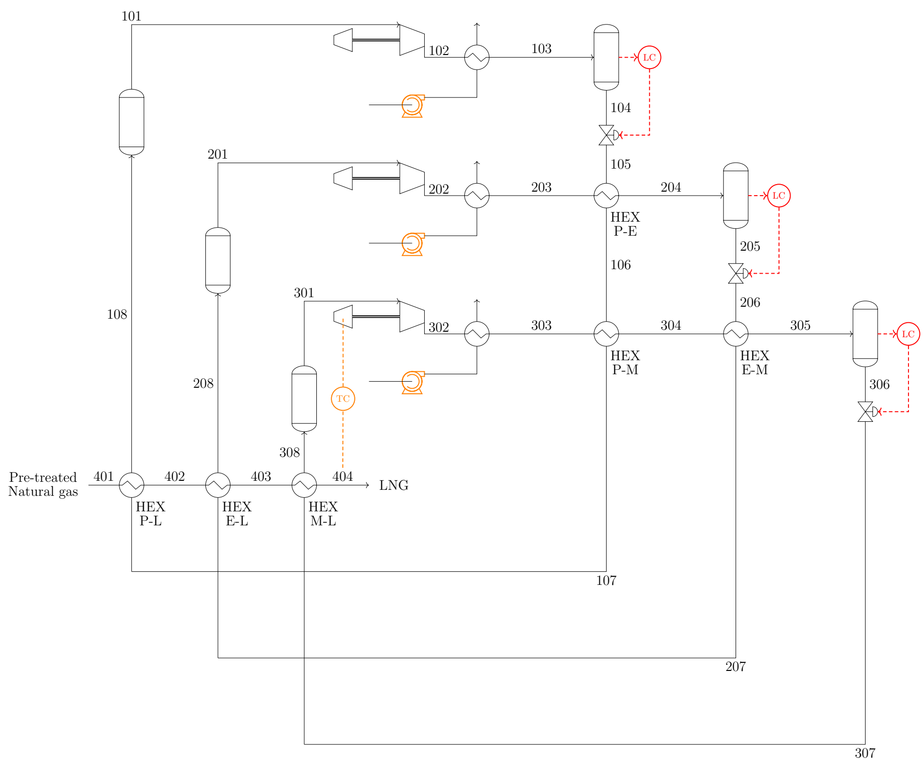

Figure 5: Illustration of stabilizing control and active constraint control structures. Stabilizing control loops are shown in red and active constraint control loops are shown in orange. (3 condenser duties at max flow, and LNG outlet temperature controller)

5.2. Control structure design for unconstrained degrees of freedom

In this section we consider how the two degrees of freedom remaining after controlling the active constraints can be used to optimize the plant performance. We devise four control structures; control structure 1 is a "standard" temperature control, whereas control structures 2, 3 and 4 are self-optimizing control structures where we control linear combinations of plant measurements. In control structure 2 we use two plant measurements, and in control structures 3 and 4 we use eight measurements. The difference between control structures 3 and 4 is that while control structure 3 only uses plant measurements, control structure 4 includes measurements of the disturbances as well, as discussed in Sec. 2.3. There are a total of 49 measurement candidates, primarily temperature-, pressure- and flow measurements, which we can use to construct the linear combinations for self-optimizing control.

As discussed in Sec. 2.4, the number of measurements in the self-optimizing control structure should be limited to avoid unnecessary expense and complexity. Ideally, a cost-benefit-analysis should be performed to find the optimal instrumentation for the plant. Fig. 6 shows the average loss for the best set of n measurements for SOC structures. A large reduction in average loss is seen when using three or more measurements. It was decided that eight measurements would give a reasonable trade-off between average loss and complexity/cost, which is why it was chosen to use eight measurements when comparing control structures 3 and 4 in the following sections. Furthermore, we observe that disturbance measurements are not included in the measurement subset unless seven or more measurements are used. "Regular" plant measurements are preferred, as they can be used to infer information about more than one disturbance.

We construct the scaling matrix $\mathbf{W_{n_y}}$ assuming that the noise of each measurement is 1% of its nominal value, with the exception of temperature and pressure measurements. For all temperature measurements we assumed that the magnitude of the noise is 1 °C. For all pressure measurements, we assumed that the noise has a magnitude of 0.2 bar for pressures on the low pressure side

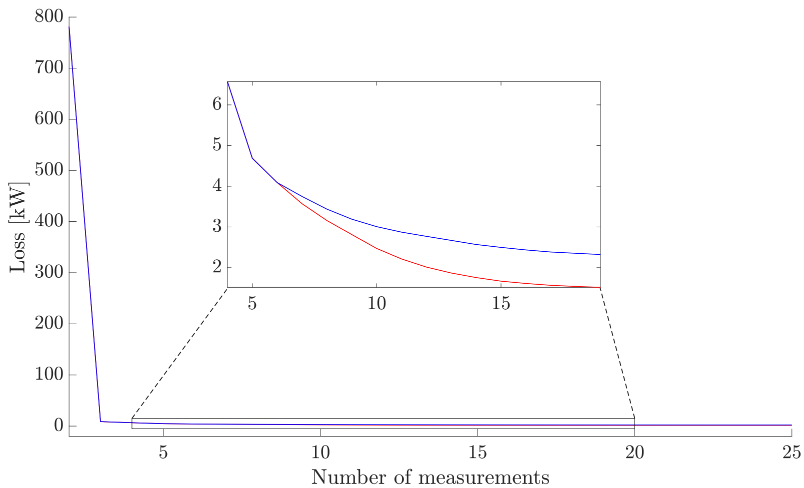

Figure 6: Average loss vs. number of measurements for a combination of plant measurements (control structure 2) shown in red and a combination of plant- and disturbance measurements (control structure 3) in blue.

of the cycle and 1 bar for pressures on the high pressure side of the cycle.

5.3. Control structure 1: "Standard" temperature control

One of the simplest operational strategies is single input - single output (SISO) feedback temperature control. Controlling the LNG outlet temperatures from the evaporators, as well as the condenser temperatures, is an intuitive way to control the process [25]. The selection matrix $\mathbf{H}$ will in that case be

$$\mathbf{H}_1 = \begin{bmatrix} 1 & 0 \\ 0 & 1 \end{bmatrix} \tag{53}$$

with

$$\mathbf{y}_1 = \begin{bmatrix} T_{402} & T_{403} \end{bmatrix}^\intercal . \tag{54}$$

It can be imagined that keeping the temperatures at predefined set-points may be sub-optimal in the event of e.g. loss of efficiency in one of the cycles. Additionally, fixing the outlet temperature from each LNG heat exchanger means that we lose operational flexibility in terms of how to distribution the load between the three cycles. Nevertheless, this strategy is expected to give acceptably small losses if the disturbances are reasonably small [25]. For larger disturbances, this control structure is expected to be sub-optimal or even infeasible. We calculate the average loss of this control structure using (18), giving

$$L_{avg.,1} = 1710.4\,\mathrm{kW}. \tag{55}$$

This average loss is about twice the loss expected for a control structure with two plant measurements, as seen from Fig. 3.

An illustration of the proposed control structure is shown in Fig. 7. In the proposed control structure, the choke at the outlet of the receiver tanks is used to control one of the corresponding receiver level, the condenser duty is maximized, and the compressor is used to control the evaporator outlet temperature. The controller pairing is based on the "pair-close" rule of thumb, but is confirmed by calculating the steady-state RGA of system [29]:

$$RGA_1 = \begin{bmatrix} \mathbf{1.0108} & -0.0108 \\ -0.0108 & \mathbf{1.0108} \end{bmatrix}. \tag{56}$$

From the RGA it is clear that a diagonal pairing should be choosen, i.e.

$$u^{cond.}_{C_3H_8} \quad \rightarrow \quad T_{103} \tag{57a}$$

$$u^{cond.}_{C_2H_6} \quad \rightarrow \quad T_{203} \tag{57b}$$

5.4. Control structure 2: Controlling a combination of two plant measurements

Using the branch and bound algorithm by Kariwala et al. [17], we can find the combination of two measurements which give the lowest average loss. These two measurements are found to be

$$\mathbf{y}_2 = \begin{bmatrix} T_{104} & P_{302} \end{bmatrix}^\mathsf{T}, \tag{58}$$

with the corresponding measurement selection matrix

$$\mathbf{H}_2 = \begin{bmatrix} 1 & 0 \\ 0 & 1 \end{bmatrix} \tag{59}$$

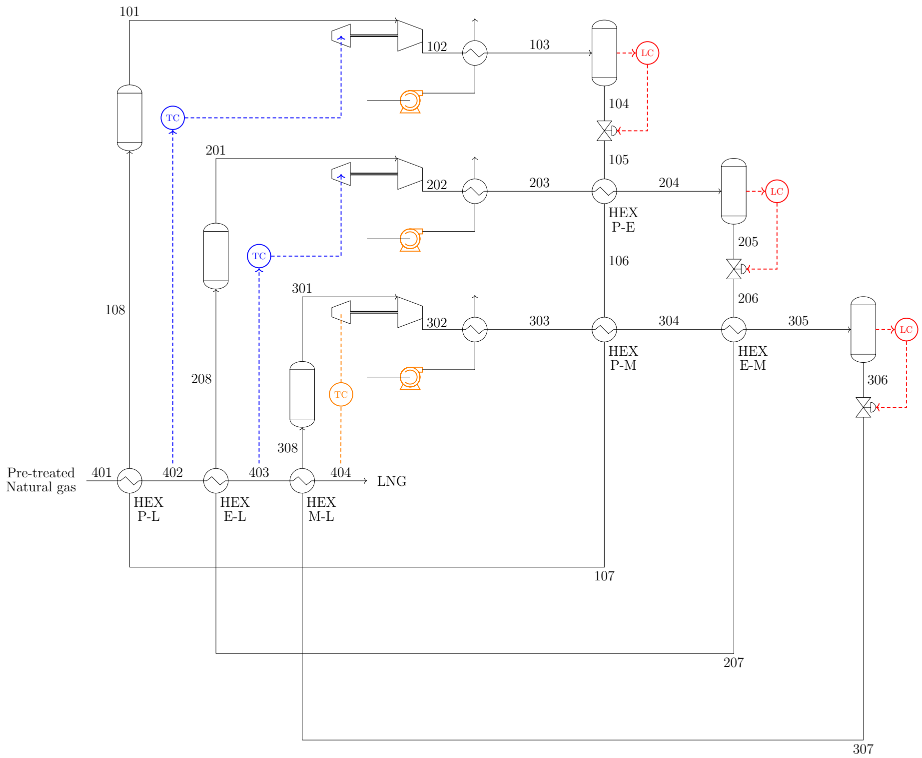

Figure 7: Illustration of proposed control structure 1. Stabilizing control loops are shown in red, active constraint control loops are shown in orange and optimizing control loops are shown in blue.

Using (18), this control structure results in an average local loss of

$$L_{avg.,2} = 781.3\,\mathrm{kW}. \tag{60}$$

The controller pairings are found from the RGA:

$$RGA_2 = \begin{bmatrix} \mathbf{1.010} & -0.010 \\ -0.010 & \mathbf{1.010} \end{bmatrix}, \tag{61}$$

from which we get the following

$$u^{cond.}_{C_3H_8} \rightarrow H(1) \tag{62a}$$

$$u^{cond.}_{C_2H_6} \rightarrow H(2). \tag{62b}$$

5.5. Control structure 3: Controlling a combination of eight plant measurements

A combination of measurements may result in a better performing control structure, as discussed in Sec. 2. An illustration of the resulting MIMO control structure is shown in Fig. 8.

5.5.1. Optimal measurement selection

Using the branch and bound algorithm by Kariwala et al. [17], we can find the combination of eight measurements which give the lowest average loss. These eight measurements are found to be

$$\mathbf{y}_3 = \begin{bmatrix} T_{202} & T_{203} & P_{205} & P_{206} & T_{304} & P_{304} & W_{comp,E} & W_{comp,M} \end{bmatrix}^{\mathsf{T}}, \tag{63}$$

with the corresponding measurement selection matrix

$$\mathbf{H}_3 = \begin{bmatrix} 0.120 & 0.042 & -0.824 & -3.210 & 0.087 & -0.010 & 0.557 & 0.457 \\ 0.247 & 0.088 & -0.286 & -7.457 & -0.117 & -0.100 & 0.720 & -1.047 \end{bmatrix} \tag{64}$$

Note that we have scaled the variables in the model to avoid ill-conditioned matrices. In the above $\mathbf{H}$ matrix, and all subsequent $\mathbf{H}$ matrices, the temperature are in $\mathrm{K} \cdot 10^2$, the pressures are in $\mathrm{bar} \cdot 10^1$, and the compressor duties are in $\mathrm{MW} \cdot 10^2$.

Using (18), this control structure results in an average local loss of

$$L_{avg.,3} = 3.438\,\mathrm{kW}. \tag{65}$$

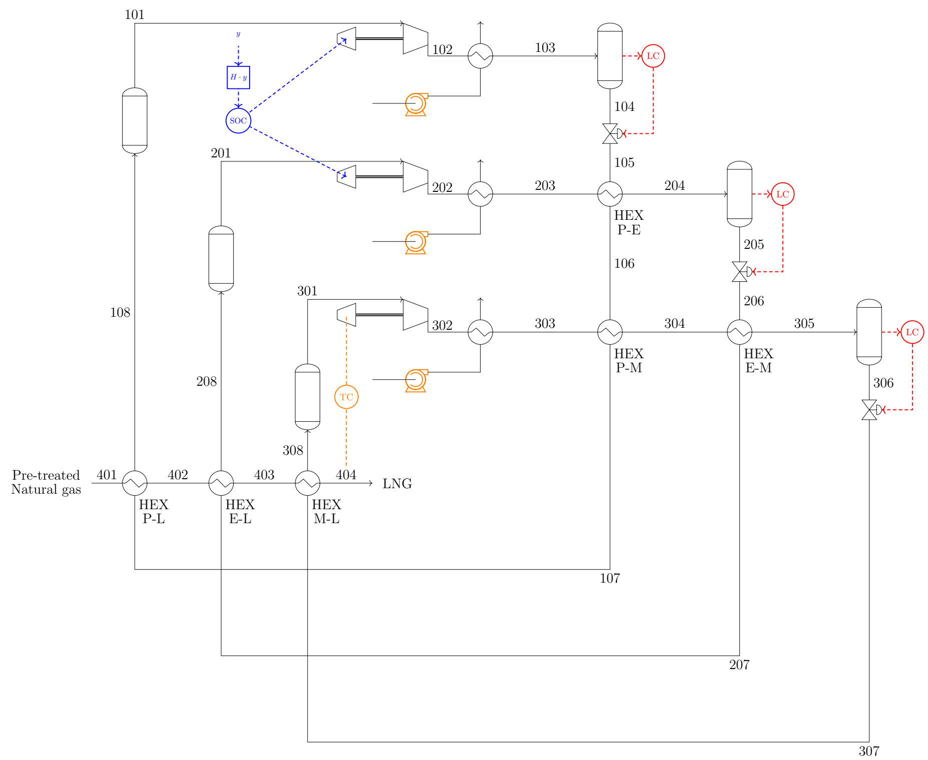

Figure 8: Illustration of proposed control structures 2, 3 & 4. The self-optimizing control structure uses plant measurements y to find the appropriate control actions for the two compressors speeds. Stabilizing control loops are shown in red, active constraint control loops are shown in orange and optimizing control loops are shown in blue.

The controller pairings are found from the RGA:

$$RGA_3 = \begin{bmatrix} \mathbf{1.2311} & -0.2311 \\ -0.2311 & \mathbf{1.2311} \end{bmatrix}, \tag{66}$$

from which we get the following

$$u^{cond.}_{C_3H_8} \quad \rightarrow \quad H(1) \tag{67a}$$

$$u^{cond.}_{C_2H_6} \quad \rightarrow \quad H(2). \tag{67b}$$

5.6. Control structure 4: Controlling a combination of plant- and disturbance measurements

Using the branch and bound algorithm once more, this time also including disturbance measurements, we find that the measurements

$$\mathbf{y}_4 = \begin{bmatrix} P_{205} & P_{206} & P_{304} & W_{comp,P} & W_{comp,E} & W_{comp,M} & UA_{cond,P} & UA_{cond,M} \end{bmatrix}^{\mathsf{T}} \tag{68}$$

result in the lowest average loss. When compared to control structure 3, we see that control structure 4 contains a different set measurements. Notably we now have a measurement of the disturbances $UA_{cond,P}$ and $UA_{cond,M}$. Note that these "measurements" are really non-linear soft-sensor estimates of the disturbances, since it is not possible to measure them directly, on-line. Due to the inclusion of the disturbance measurements, control structure 4 is expected to reject these disturbances more efficiently, thus reducing the average loss. The measurement selection matrix is

$$\mathbf{H}_4 = \begin{bmatrix} 1 & 0 & -0.0629 & -0.4587 & -0.2348 & -1.4381 & -0.0463 & 0.0304 \\ 0 & 1 & 0.0139 & 0.0100 & -0.1082 & 0.1375 & 0.0001 & -0.0034 \end{bmatrix} \tag{69}$$

Using (18), this control structure results in an average local loss of

$$L_{avg.,4} = 3.158\,\mathrm{kW}, \tag{70}$$

which is slightly lower than that of control structure 3, due to the ability to detect and reject changes in the condenser efficiencies more efficiently.

The controller pairings are found from the RGA:

$$RGA_4 = \begin{bmatrix} \mathbf{1.1267} & -0.1267 \\ -0.1267 & \mathbf{1.1267} \end{bmatrix}, \tag{71}$$

from which we get a diagonal pairing

$$u^{cond.}_{C_3H_8} \quad \rightarrow \quad H(1) \tag{72a}$$

$$u^{cond.}_{C_2H_6} \quad \rightarrow \quad H(2). \tag{72b}$$

6. Comparison control structures

6.1. Steady-state losses for larger disturbances in a dynamic simulation

Fig. 9 shows the performance of the four control structures in terms of their steady-state losses for four disturbances, evaluated on the nonlinear model. The self-optimizing control structures clearly outperform the simple temperature control structure. We also observe that control structure 3 and 4 perform about equally well, with both giving very small losses for most disturbances. Note that disturbances in the LNG flow rate are expected to result in significantly higher losses than the other disturbances. This is reasonable, since the load directly influences the energy consumption. Control structures 3 and 4 give much lower losses than control structures 1 and 2 for this disturbance, which significantly impacts the expected average loss.

6.2. Comparison of closed-loop responses

Fig. 10 shows the performance of the four control structures in terms of their closed-loop responses or a dynamic simulation to selected disturbances. Again, it can be seen that the SOC structures outperform control structure 1 in terms of the steady-state losses. All responses can be seen to be quite slow, with a time constant of around 50 seconds. The hold-ups of the tanks were chosen quite large, which leads to the slow responses.

We observe that the SOC structures have slightly higher transient losses, before settling at lower steady-state losses. The transient losses are not optimized by regular self-optimizing control, as self-optimizing control is inherently

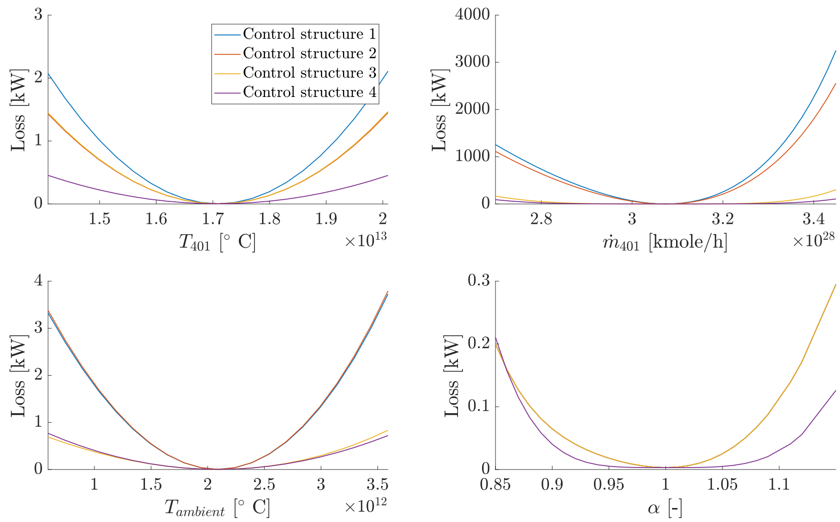

Figure 9: Steady state losses for the three different control structures: control structure 1 in blue, control structure 2 in red, control structure 3 in yellow and control structure 4 in purple. Note the difference in scales.

a steady-state method. Although the extension of SOC to dynamic problems has been attempted by some authors, it is currently an immature research field [10] and falls outside the scope of this paper. It should also be noted that even though the transient losses can be negative (as illustrated in Fig. 10), the steady-state losses can not. This is because strictly speaking, the loss is defined in terms of the steady-state value alone.

7. Discussion and conclusion

In this paper we investigated the possibilities of applying self-optimizing control to an LNG liquefaction plant. After implementing a model of the plant, we found the optimal operating point by minimizing the energy consumption of the compressors, subject to operational constraints. At the nominal operating point it was found that the minimum outlet temperature specification was active in addition to the maximum condenser duties, which left us with two degrees

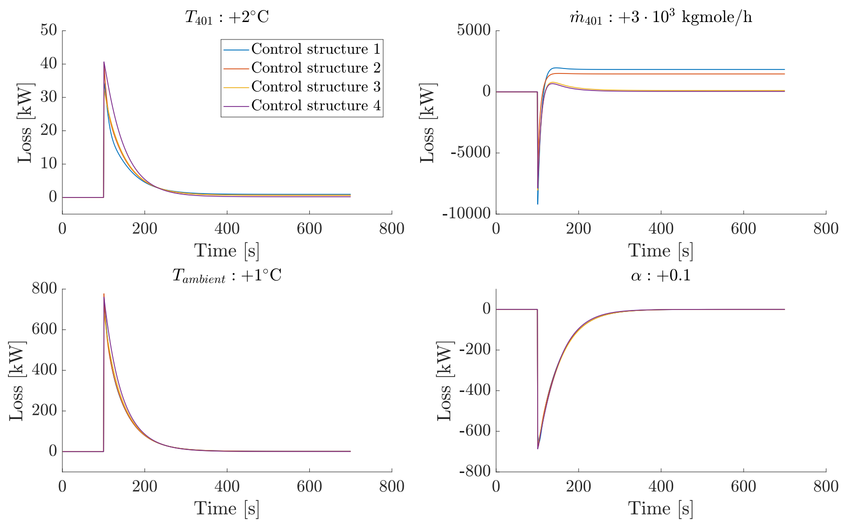

Figure 10: Closed-loop responses of the four control structures to selected disturbances.

of freedom for optimizing operation after controlling the levels and the active constraints.

We implemented four different control strategies which utilized these degrees of freedom to achieve self-optimizing control. The first control strategy was to keep the LNG temperatures at the outlet of the evaporators constant at their nominal operating points. This strategy resulted in relatively large steady state losses.

The second control structure was based on controlling a linear combination of variables to a set-point. We first identified the optimal subset of two plant measurements, and then found the combination matrix $\mathbf{H}$ using the exact local method. This self-optimizing control strategy showed significantly better performance than the constant-temperature-policy. The third control structure is similar to the second, but instead of using only two plant measurements, this control structured used eight plant measurements in $\mathbf{H}$. We observed that these additional measurements lowered the average steady-state losses significantly.

The final control structure is similar to the third, with the only difference being that we now include measurements of the disturbances in addition to the plant measurements. Due to the inclusion of disturbance measurements, the fourth control structure gave slightly lower steady-state losses than the third control structure for the same number of measurements, both in terms of the average local losses and the global losses for selected (large) disturbances. However, it seems that including measured disturbances does not significantly improve operation in this case (compared to the improvement of using eight instead of two measurements).

Acknowledgments

Financial support by SUBPRO is gratefully acknowledged

References

[1] B. Austbø, S. W. Løvseth, T. Gundersen, Annotated bibliography - Use of optimization in LNG process design and operation, Computers & Chemical Engineering 71 (2014) 391–414.

[2] M. Grötschel, S. Krumke, J. Rambau, Online Optimization of Large Scale Systems.

[3] M. Ellis, H. Durand, P. D. Christofides, A tutorial review of economic model predictive control methods, Journal of Process Control 24 (8) (2014) 1156 – 1178.

[4] L. F. S. Larsen, Model Based Control of Refrigeration Systems, Ph.D. thesis, Aalborg University (2006).

[5] D. Leducq, J. Guilpart, G. Trystram, Non-linear predictive control of a vapour compression cycle, International Journal of Refrigeration 29 (5) (2006) 761–772.

[6] L. F. Larsen, R. Izadi-Zamanabadi, R. Wisniewski, Supermarket Refrigeration System - Benchmark for Hybrid System Control, in: Proc. of European Control Conference, 2007.

[7] D. Sarabia, F. Capraro, L. F. Larsen, C. De Prada, Hybrid Control of a Supermarket Refrigeration Systems, in: Proc. of American Control Conference, IEEE, 2007, pp. 4178–4185.

[8] T. G. Hovgaard, L. F. Larsen, K. Edlund, J. B. Jørgensen, Model predictive control technologies for efficient and flexible power consumption in refrigeration systems, Energy 44 (1) (2012) 105–116.

[9] S. Skogestad, Plantwide control: The search for the self-optimizing control structure, Journal of Process Control 10 (5) (2000) 487 – 507.

[10] J. Jäschke, Y. Cao, V. Kariwala, Self-Optimizing Control–A Survey, Annual Reviews in Control 43 (2017) 199–223.

[11] A. Verheyleweghen, J. Jäschke, Self-Optimizing Control of a Two-Stage Refrigeration Cycle, IFAC-PapersOnLine 49 (7) (2016) 845–850.

[12] J. B. Jensen, S. Skogestad, Optimal operation of a mixed fluid cascade LNG plant, Computer Aided Chemical Engineering 21 (2006) 1569–1574.

[13] A. Singh, M. Hovd, V. Kariwala, Controlled Variables Selection for Liquefied Natural Gas Plant, IFAC Proceedings Volumes 41 (2) (2008) 13913–13918.

[14] F. A. Michelsen, B. F. Lund, I. J. Halvorsen, Selection of optimal, controlled variables for the TEALARC LNG process, Industrial & Engineering Chemistry Research 49 (18) (2010) 8624–8632.

[15] V. Alstad, S. Skogestad, E. S. Hori, Optimal measurement combinations as controlled variables, Journal of Process Control 19 (1) (2009) 138–148.

[16] J. Jäschke, S. Skogestad, Optimal Operation by Controlling the Gradient to Zero, in: Proc. of 18th IFAC World Congress, IFAC, 2011, pp. 6073–6078.

[17] V. Kariwala, Y. Cao, Bidirectional branch and bound for controlled variable selection. Part II: Exact local method for self-optimizing control, Computers & Chemical Engineering 33 (8) (2009) 1402 – 1412.

[18] I. J. Halvorsen, S. Skogestad, J. C. Morud, V. Alstad, Optimal Selection of Controlled Variables, Industrial & Engineering Chemistry Research 42 (14) (2003) 3273–3284.

[19] V. Kariwala, Y. Cao, S. Janardhanan, Local Self-Optimizing Control with Average Loss Minimization, Industrial & Engineering Chemistry Research 47 (4) (2008) 1150–1158.

[20] R. Yelchuru, S. Skogestad, MIQP formulation for Controlled Variable Selection in Self Optimizing Control, IFAC Proceedings Volumes 43 (5) (2010) 61–66.

[21] D. Andress, R. Watkins, J. Waynert, J. Barclay, S. Breon, E. Daly, J. Demko, M. DiPirro, J. R. Hull, P. J. Kelley, et al., Beauty of Simplicity: Phillips Optimized Cascade LNG Liquefaction Process, in: AIP Conference Proceedings, Vol. 710, AIP, 2004, pp. 91–100.

[22] E. Lemmon, R. Jacobsen, S. Penoncello, S. Beyerlein, Computer Programs for the Calculation of Thermodynamic Properties of Cryogens and other Fluids, in: P. Kittel (Ed.), Advances in Cryogenic Engineering, Vol. 39 of Advances in Cryogenic Engineering, Springer US, 1994, pp. 1891–1897.

[23] P. Dranchuk, H. Abou-Kassem, Calculation of Z Factors For Natural Gases Using Equations of State, Journal of Canadian Petroleum Technology 14 (03).

[24] J. B. Jensen, S. Skogestad, Optimal operation of simple refrigeration cycles: Part I: Degrees of freedom and optimality of sub-cooling, Computers & Chemical Engineering 31 (5) (2007) 712–721.

[25] J. B. Jensen, S. Skogestad, Optimal operation of simple refrigeration cycles: Part ii: Selection of controlled variables, Computers & Chemical Engineering 31 (12) (2007) 1590–1601.

[26] J. Andersson, A General-Purpose Software Framework for Dynamic Optimization, PhD thesis, Arenberg Doctoral School, KU Leuven, Department of Electrical Engineering (ESAT/SCD) and Optimization in Engineering Center, Kasteelpark Arenberg 10, 3001-Heverlee, Belgium (October 2013).

[27] L. T. Biegler, Nonlinear Programming: Concepts, Algorithms, and Applications to Chemical Processes, Vol. 10, SIAM, 2010.

[28] E. M. B. Aske, S. Skogestad, Consistent Inventory Control, Industrial & Engineering Chemistry Research 48 (24) (2009) 10892–10902.

[29] S. Skogestad, I. Postlethwaite, Multivariable Feedback Control: Analysis and Design, Vol. 2, Wiley New York, 2007.

AppendixA. Design parameters

Table A.4: Design parameters for calculating the saturation temperature in (26)

Parameter	Value		
	Propane	Ethane	Methane
$c_{T_{\mathrm{sat},i},0}$	3.0053	2.4141	1.4966
$c_{T_{\mathrm{sat},i},1}$	0.93582	0.77135	0.51530
$c_{T_{\mathrm{sat},i},2}$	0.24817	0.21080	0.13110

Table A.5: Design parameters for calculating the specific liquid saturation enthalpy in (27)

Parameter	Value		
	Propane	Ethane	Methane
$c_{\hat{H}_{\mathrm{liq},i},0}$	-9992.7	-9447.4	-15187
$c_{\hat{H}_{\mathrm{liq},i},1}$	15991	12605	5974.2
$c_{\hat{H}_{\mathrm{liq},i},2}$	-11110	-12132	-5488.7
$c_{\hat{H}_{\mathrm{liq},i},3}$	4838.4	7061.9	3138.6
$c_{\hat{H}_{\mathrm{liq},i},4}$	-970.54	-2146.5	-943.33
$c_{\hat{H}_{\mathrm{liq},i},5}$	50.621	319.1	138.42
$c_{\hat{H}_{\mathrm{liq},i},6}$	4.8879	-18.124	-7.6457

Table A.6: Design parameters for calculating the vapor saturation enthalpy in (28)

Parameter	Value		
	Propane	Ethane	Methane
$c_{\hat{H}_{\mathrm{vap},i},0}$	9036.9	5906	-6622.6
$c_{\hat{H}_{\mathrm{vap},i},1}$	11005	6200.8	2117.7
$c_{\hat{H}_{\mathrm{vap},i},2}$	-12980	-7884.9	-1650.9
$c_{\hat{H}_{\mathrm{vap},i},3}$	9271.9	5412.9	518.47
$c_{\hat{H}_{\mathrm{vap},i},4}$	-3644.6	-1973	-59.04
$c_{\hat{H}_{\mathrm{vap},i},5}$	721.52	356.06	0
$c_{\hat{H}_{\mathrm{vap},i},6}$	-56.405	-25.103	0

Table A.7: Design parameters for calculating the heat capacity in (29)

Parameter	Value		
	Propane	Ethane	Methane
$c_{C_{p,i},1}$	1.702	1.131	1.213
$c_{C_{p,i},2}$	$9.081 \cdot 10^{-3}$	$19.225 \cdot 10^{-3}$	$28.785 \cdot 10^{-3}$
$c_{C_{p,i},3}$	$-2.164 \cdot 10^{-6}$	$-5.561 \cdot 10^{-6}$	$-8.824 \cdot 10^{-6}$

Table A.8: Design parameters for calculating the compressibility factor in (30)

Parameter	Value
$c_{Z_i,1}$	0.3265
$c_{Z_i,2}$	-1.0700
$c_{Z_i,3}$	-0.5339
$c_{Z_i,4}$	0.01569
$c_{Z_i,5}$	-0.05165
$c_{Z_i,6}$	0.5475
$c_{Z_i,7}$	-0.7361
$c_{Z_i,8}$	0.1844
$c_{Z_i,9}$	0.1056
$c_{Z_i,10}$	0.6134
$c_{Z_i,11}$	0.7210

Table A.9: Design parameters for calculating the compressor efficiency in (38)

Parameter	Value		
	Propane	Ethane	Methane
$c_{\eta_i,1}$	0.061733	0.03448682	0.0251571
$c_{\eta_i,2}$	-0.074	-0.074	-0.074
$c_{\eta_i,3}$	0.338767	0.18925109	0.138053
$c_{\eta_i,4}$	6.5963	6.5963	6.5963

Table A.10: Design parameters for calculating the polytropic head in (39)

Parameter	Value		
	Propane	Ethane	Methane
$c_{comp,1}$	1.79	1.79	1.79
$c_{comp,2}$	1.9928	1.9928	0.27146
$c_{comp,3}$	35.1962	63.00	11.765
$c_{comp,4}$	18.3546	32.855	45.040

Table A.11: Design parameters for calculating the polytropic head in (41)

Parameter	Value		
	Propane	Ethane	Methane
$c_{h_{poly,scaled,i},1}$	2.11	2.11	2.11

Table A.12: Design parameters for calculating the molar flow through the valve in (42)

Parameter	Value		
	Propane	Ethane	Methane
$c_{choke,i}$	13.0	8.4	3.4